Springer

Journal of Mechanical Science and Technology 23 (2009) 2030~2037

Journal of Mechanical Science and Technology

www.springerlink.com/content/1738-494x
DOI 10.1007/s12206-009-0436-y

A path tracking control algorithm for underwater mining vehicles †

Sup Hong[1], Jong-Su Choi[1], Hyung-Woo Kim[1], Moon-Cheol Won[2,*], Seung-Chul Shin[2], Joon-Seong Rhee[2] and Hyo-un Park[2]

[1]*Ocean Development System Division, MOERI/KORDI, 171 Jang-Dong, Yuseong-Gu, Daejeon 305-764, Korea*
[2]*Department of Mechatronics Engineering, Chungnam National University, 220 Gung-dong, Yuseong-Gu, Daejeon 305-764, Korea*

(Manuscript Received January 23, 2008; Revised July 7, 2008; Accepted April 13, 2009)

Abstract

In this paper, a path tracking control algorithm is formulated for the use of tracked underwater mining vehicles. The algorithm consists of two parts, the forward velocity control and the heading angle control. The control algorithm is designed based on kinematics, and it considers the track slips and the longitudinal and yaw dynamic models of the tracked vehicle including the soil–track interaction force model. The desired heading angle is obtained by the so-called "Line of Sight" method. The suggested algorithm is tested by numerical simulations using the TRACSIM software developed by MOERO/KORDI, Korea. After the control gains are tuned by a series of numerical simulations, the algorithm is verified on a scale vehicle on air on a soil bin test bed containing the cohesive soil of the Bentonite-water mixture.

Keywords: Tracked vehicle; Control; Underwater mining

1. Introduction

Commercial deep underwater mining is expected to be realized in the near future because of the depletion of land mining resources. As a method for deep underwater mining, mining research using a tracked vehicle system has been conducted in many countries including Germany, U.S.A, China, and Korea [1]. The tracked vehicle is operated on an extremely soft cohesive soil to excavate the valuable metals such as manganese, and send the metals to the surface ships through piping systems. In this situation, the vehicle can experience large slips on its tracks. Also, the underwater piping systems attached to the vehicle induce large disturbance forces and cause additional slip to the vehicle. The vehicle should then have the capability to follow the desired mining trajectories under these disturbance forces. Therefore, it is very important to have a good tracking control algorithm which takes into account the potentially large slips on the tracks.

Previous works [2, 3] on controlling tracked vehicles focused only on vehicles operating on land. The dynamic model of the tracked vehicle is difficult to operate because of the complex and nonlinear soil-track interaction phenomenon [4, 5]. In this regard, the current study therefore focuses on the design of a tracking control algorithm that considers the large track slip for such tracked vehicles, and performs verification by experiments using a model scale vehicle. The designed control algorithm is based on the simplified kinematics and dynamics of the tracked vehicle. The designed tracking control algorithm is verified by numerical simulation followed by experimental verification using a model scale vehicle. This vehicle is operated by two BLDC motors and is equipped with in-vehicle sensors such as track encoders and rate gyro sensors. A vision system is used for

† This paper was recommended for publication in revised form by Associate Editor Kyongsu Yi

*Corresponding author. Tel.: +82 42 821 6875, Fax.: +82 42 823 4919
E-mail address: mcwon@cnu.ac.kr

the absolute location information of the vehicle instead of a sonar system such as the Long Base Line (LBL) or Super Short Base Line (SSBL).

2. Mathematical modeling of the tracked vehicle

We assume that the vehicle operates on a plat with 2-D surfaces. In addition, it is assumed that the turning motion is not severe, and the resulting centrifugal forces are relatively small. In this case, the motion of the tracked vehicle can be represented by three degrees of freedom (x, y, ψ), where (x, y) represents the coordinate of the mass center of the vehicle, and ψ represents the heading angle of the vehicle as shown in Fig. 1.

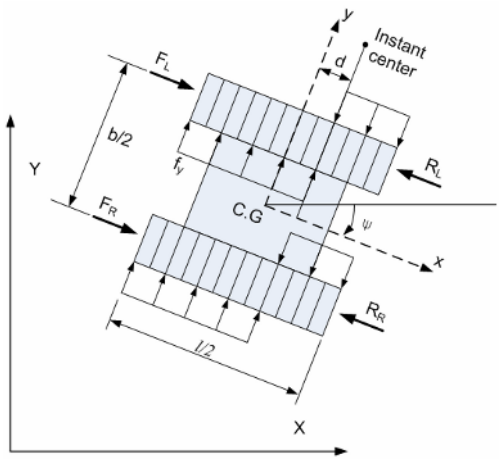

Fig. 1. Definitions of the coordinates and forces on the tracked vehicle.

In Fig. 1, the (X, Y) coordinate represents a fixed global coordinate, and the (x, y) coordinate represents a moving coordinate attached to the mass center of the vehicle. The dynamic equation of the vehicle can be represented by Eqs. (1)-(3) [2].

$$M\ddot{x} = F_L + F_R - R_L - R_R \tag{1}$$

$$M\ddot{y} = 4 f_y d \tag{2}$$

$$I\ddot{\psi} = (F_R - R_R)b - (F_L - R_L)b - 2 f_y (l^2 - d^2) \tag{3}$$

The definitions of the variables used in Eqs. (1)-(3) are as follows:

F_L, F_R : Tracktive forces on the left and right tracks
R_L, R_R : Resistance forces on the left and right tracks
f_y : Lateral resistance force on each track
d : The distance between the mass center and the instantaneous rotation center of the vehicle
M : Vehicle mass
I : Mass moment of inertia of the vehicle
b : Half of the distance between each track's center line
l : Half of the vehicle length

From the kinematics of the vehicle, the left and right track slips can be defined by Eq. (4) and Eq. (5).

$$i_L = \frac{r\omega_L - (\dot{x} - b\dot{\psi})}{r\omega_L} \tag{4}$$

$$i_R = \frac{r\omega_R - (\dot{x} + b\dot{\psi})}{r\omega_R} \tag{5}$$

Here, ω_L and ω_R are the angular velocities of the sprockets on the left and the right tracks, and r is the radius of the sprocket. Also, the relation between the track slip and the tracktive force can be approximated by Eq. (6) [4].

$$F = F_{\max}\left[1 - \frac{\alpha}{|i|}(1 - e^{-|i|\alpha})\right] sign(i) \tag{6}$$

Here, $F_{\max}$ is the maximum tracktive force, α is the parameter representing the characteristics of the soil property, and i is the track slip.

3. Tracking control algorithm

Typical nonlinear tracking control methods [6] try to locate the vehicle on the $(x_d(t), y_d(t), \psi_d(t))$ coordinate for a given time t, where $(x_d(t), y_d(t), \psi_d(t))$ is the desired vehicle location and heading angle. These kinds of control algorithms can be inadequate for mining vehicle applications since the large disturbances and insufficient tracktive forces from the soil can make the task impossible. Instead of the typical tracking control methods (position tracking combined with a heading angle control algorithm), this study suggests a forward velocity tracking algorithm to guide the vehicle on a desired path.

The desired velocity and heading angle are calculated based on way points and the Line of Sight (LOS) concept [7]. The way points comprise the desired (x, y) position coordinate, and the lines that connect the way points comprise the desired vehicle trajectory as shown in Fig. 2. We also assign a desired velocity of the vehicle on the waypoint as v_i on each (x_i, y_i).

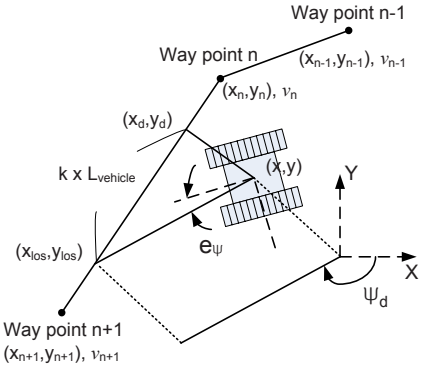

Fig. 2. Definition of the LOS vector.

The desired vehicle velocity for a vehicle at $(x,\ y)$ is obtained as follows. First, we find the nearest point (x_d, y_d) on the desired trajectory from the vehicle mass center, which can be found by using the parameter u in Eqs. (7)-(9). This parameter indicates how far (x_d, y_d) is located from (x_n, y_n).

$$u = \frac{(x - x_n)(x_{n+1} - x_n) + (y - y_n)(y_{n+1} - y_n)}{d_n^2} \quad (7)$$

Here, d_n is the distance between way point n and way point $n+1$.

$$x_d = x_n + u(x_{n+1} - x_n) \quad (8)$$

$$y_d = y_n + u(y_{n+1} - y_n) \quad (9)$$

The desired velocity v_d is defined by Eq. 10, which is a linear interpolation of v_n and v_{n+1}.

$$v_d = v_n + u(v_{n+1} - v_n) \quad (10)$$

The desired heading angle is defined by using the LOS concept. The desired heading point (x_{LOS}, y_{LOS}) on the desired trajectory is defined as the point located at the distance of $K \cdot L$ from (x_d, y_d), where the constant K is a LOS constant, and L is the vehicle length. The desired heading angle is defined as the phase angle of the vector connecting (x_d, y_d) and (x_{LOS}, y_{LOS}), and calculated by Eq. (11).

$$\psi_d = \arctan\left(\frac{y_{LOS} - y}{x_{LOS} - x}\right) \quad (11)$$

We define the velocity error e_v using Eq. (12) and the heading angle error e_ψ using Eq. (13).

$$e_v = v_d - v \quad (12)$$

$$e_\psi = \psi_d - \psi \quad (13)$$

To make the two errors become zero, the desired closed loop error dynamics can be designed using Eq. (14) and Eq. (15).

$$\dot{e}_v + k_{vP} e_v + k_{vI} \int e_v dt = 0 \quad (14)$$

$$\ddot{e}_\psi + k_{\psi D} \dot{e}_\psi + k_{\psi P} e_\psi = 0 \quad (15)$$

Here, $k_{vP}, k_{vI}, k_{\psi D}$, and $k_{\psi P}$ are the positive constants which decide the locations of the closed loop poles of each dynamics.

Here, we assume that the yaw rate of the vehicle is limited to a small value. The assumption is reasonable since the vehicle does not have to perform the quick and sharp turning motions in the usual mining processes. In this case, the distance d between the mass center and the instantaneous motion center is almost zero. Also, when we assume that the turning radius is sufficiently large, the lateral resistance force f_y on each track can be negligible. Under these assumptions, Eq. (3) can be approximated to Eq. (16).

$$I\ddot{\psi} = \bar{F}_R b - \bar{F}_L b \quad (16)$$

Here, $\bar{F}_R = F_R - R_R$ and $\bar{F}_L = F_L - R_L$ are the net track forces on the left and right tracks. With these notations, Eq. (1) can be rewritten similar to Eq. (17).

$$M\ddot{x} = \bar{F}_L + \bar{F}_R \quad (17)$$

Likewise, the desired motion characteristics of the mining vehicle are not rapid in the linear velocity and heading angle change, so the changes in desired velocity and the desired heading angle $\ddot{\psi}_d$ and $\dot{v}_d$ can be neglected. In this case, Eqs. (14)-(17) yield Eq. (18) and Eq. (19), where $(\bar{F}_{L,d}, \bar{F}_{R,d})$ is the desired net forces from the left and right tracks.

$$\bar{F}_{Ld} + \bar{F}_{Rd} = M(k_{vP} e_v + k_{vI} \int e_v dt) \underline{\underline{\Delta}} \bar{F}_{\sigma d} \quad (18)$$

$$\bar{F}_{Ld} - \bar{F}_{Rd} = -\frac{I}{b}(k_{\psi D} \dot{e}_\psi + k_{\psi P} e_\psi) \underline{\underline{\Delta}} \bar{F}_{\delta d} \quad (19)$$

From Eq. (18) and Eq. (19), the desired net forces can be calculated as Eq. (20) and Eq. (21).

$$\bar{F}_{Ld} = \frac{\bar{F}_{\sigma d} + \bar{F}_{\delta d}}{2} \quad (20)$$

$$\bar{F}_{Rd} = \frac{\bar{F}_{\sigma d} - \bar{F}_{\delta d}}{2} \quad (21)$$

The desired left and right track slips $(i_{L,d}, i_{R,d})$ can be obtained from the experimental curve that relates the slip with the net track force as shown in Fig. 11. Finally, the desired track speeds are obtained as Eq.

(22) and Eq. (23) using Eq. (4) and Eq. (5).

$$\omega_{L,d} = \frac{\dot{x}_d - b\dot{\psi}_d}{r(1-i_{L,d})} \tag{22}$$

$$\omega_{R,d} = \frac{\dot{x}_d + b\dot{\psi}_d}{r(1-i_{R,d})} \tag{23}$$

Here, $\dot{x}_d = v_d$ and $\dot{\psi}_d$ can be approximately calculated from the numerical differentiation followed by a low pass filtering of ψ_d for digital implementations.

The control algorithm represented by Eq. (22) and Eq. (23) is obtained purely from the dynamic and kinematic models of the tracked vehicle. In reality, the models more often than not do not exactly match the real plan, and they involve some uncertainties. To overcome the problems caused by the incorrect models, we added a direct propositional control part in relation to the heading angle error on the model-based control scheme. The final control algorithm is represented by Eq. (24) and Eq. (25).

$$\omega_{L,d} = \frac{\dot{x}_d - b\dot{\psi}_d}{r(1-i_{L,d})} - k_\psi e_\psi \tag{24}$$

$$\omega_{R,d} = \frac{\dot{x}_d + b\dot{\psi}_d}{r(1-i_{R,d})} + k_\psi e_\psi \tag{25}$$

The block diagram representation of the algorithm is depicted in Fig. 3.

4. Numerical verification of the control algorithm

A simulation code named TRACSIM[1] developed by MOERI/KORDI, Korea is used for the verification of the control algorithm. The program can simulate six degrees of freedom motions of tracked vehicles on a soft soil. The control input for the simulations and the experiments explained in Section 5 is the left and right track speed of the vehicle. The parameters of the model scale test vehicle used in the experiments are used in the simulation as well. Table 1 shows the geometric- and mass-related parameters of the test vehicle.

Table 1. Parameters of the model scale test vehicle.

Width(B)	0.75 m	Mass	167 kg
Length(L)	0.9 m	Moment of Inertia	5988 kgm^2
Height(H)	0.4 m		

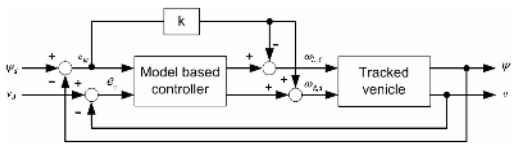

Fig. 3. Block diagram of the control algorithm.

First, open loop simulations without feedback control were carried out, and the results were compared with the experimental open loop run results. A prescheduled time history for the left and right track speed $(\omega_L(t), \omega_R(t))$ is used as the input for each simulation and experiment.

Fig. 4 shows the results of a straight run simulation and experiment. There is a 2.4 cm difference between the simulation and experiment on the final position of the vehicle with a total travel of 1.5 m. Meanwhile, Fig. 5 shows the results of the turning simulation and experiment. In this case, the track speed ratio (ω_L / ω_R) was gradually changed from 1.4 to 2.5. The simulation and experimental results match relatively well for the small speed ratio. However, for large speed ratios, the resulting trajectories show big

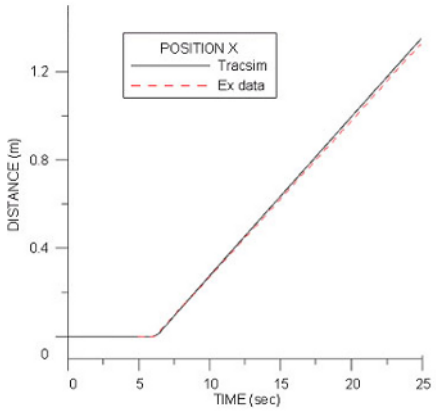

Fig. 4. Simulated experimental paths for a straight run.

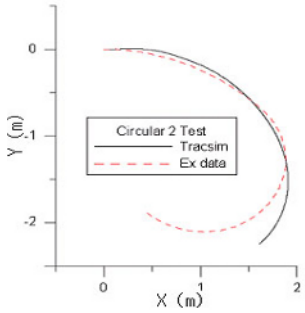

Fig. 5. Simulated experimental paths for a turning with varying track speed ratios.

Table 2. Control gains used in the simulations.

$k_{\psi D}$	0.1	$k_{\psi P}$	0.05
k_{vP}	20	k_{vI}	3
k_{ψ}	0.02	LOS	1.5

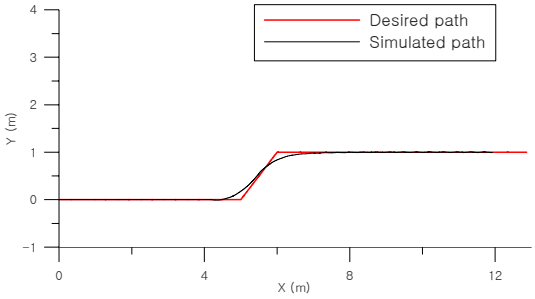

Fig. 6. Vehicle mass center trajectory of the lane change simulation result (LOS:1.5).

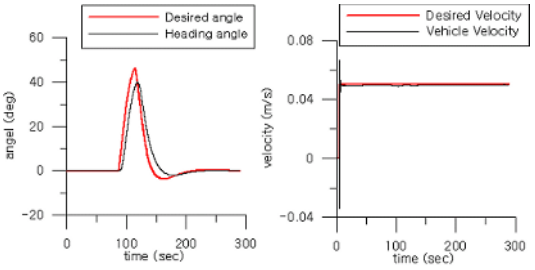

Fig. 7. Simulated results of the heading angle and the velocity response of lane change.

differences. This suggests that for the small speed ratio of less then 2.0, the simulation can predict the actual tracking behaviors.

Next, closed loop control simulations have been done. Table 2 shows the control gains used in the following three closed-loop simulations.

Fig. 6 shows the vehicle position trajectory of the lane change simulation, while Fig. 7 shows the corresponding heading angle and forward velocity histories. The desired forward velocity is $0.05m/\sec$. In this low speed, the position tracking result as well as the heading and forward velocity tracking show good performances.

Fig. 8 shows the simulated vehicle position trajectory of a circular turning followed by a lane change simulation. The desired vehicle speed is $0.1m/\sec$. The position tracking result shows bigger errors as compared to that of the low speed lane change simulation.

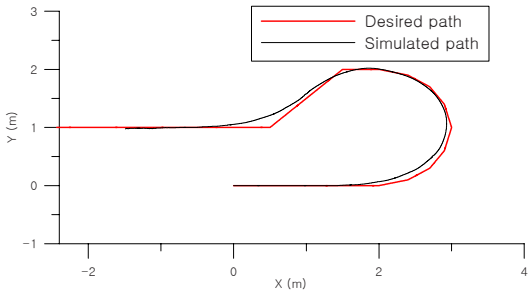

Fig. 8. Vehicle mass center trajectories of the turning and lane change simulation results.

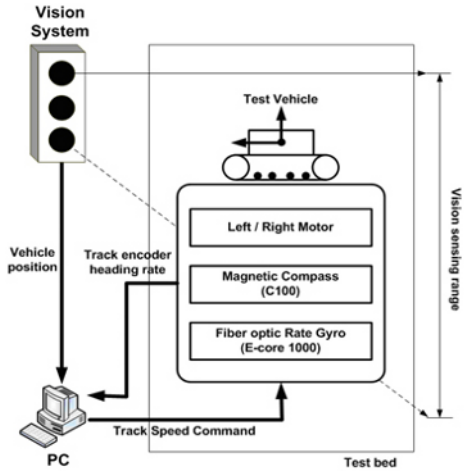

Fig. 9. Schematic diagram of the experimental set-up.

5. Experimental verification of the control algorithm

The experiments were carried out using a model scale tracked vehicle on a test bed on air. A vision system is used to replace the sonar system because of the demands of on-air experiments. Fig. 9 shows the schematic diagram of the experimental set-up. This set-up includes a model scale tracked vehicle (Fig. 10) with the geometric and weight parameters given in Table. 1, a test bed (3.7 m×6.0 m) having an extremely soft cohesive Bentonite soil, a vision system for the absolute location information of the vehicle, and a data acquisition PC system. Since the experiment was carried out on air, the effects of fluid force and buoyancy in real underwater conditions are not realized in this experimental set-up. The test vehicle is equipped with various in-vehicle sensors such as a fiber optic rate gyro and two track encoders. The vehicle tracks are operated by two BLDC motors.

Table 3. Controller gains and LOS of the experiments.

$k_{\delta 1}$	0.1	$k_{\delta 2}$	0.5
$k_{\sigma 1}$	60	$k_{\sigma 2}$	0.2
k_{ψ}	0.1	**LOS**	1

Fig. 10. Side view of the test vehicle.

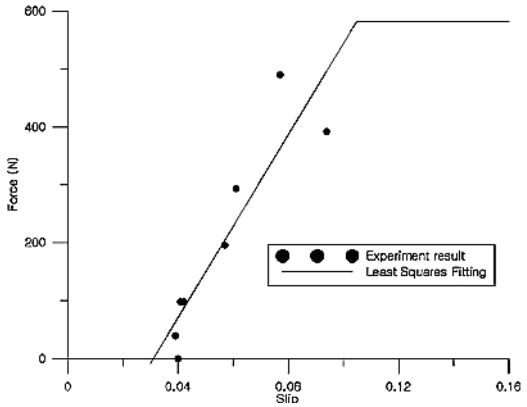

Fig. 11. Experimental result of the relationship between the net tracktive force and the slip.

Before the implementation of the control experiments, it was necessary to establish the relationship between the vehicle slip and the net forces of the vehicle tracks. To do so, the test vehicle performed several straight runs under different loading conditions. Fig. 11 shows the experimental data of the sum of the net forces from the two tracks and the corresponding linear least square fitting of the points. The measured maximum net force from the two tracks is about 589N. A slip of about 0.03 (3%) is necessary to yield a positive net force, which means that at least 3% slip is necessary for the vehicle to move. This relation is used in the control algorithm to find the desired track slip in Eq. (24) and Eq. (25).

Since the experimental result shown in Fig. 11 is

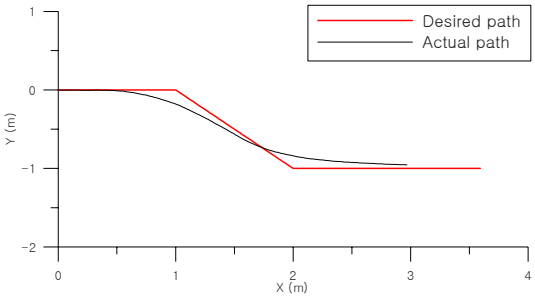

Fig. 12. Vehicle mass center trajectory of the lane change experiment.

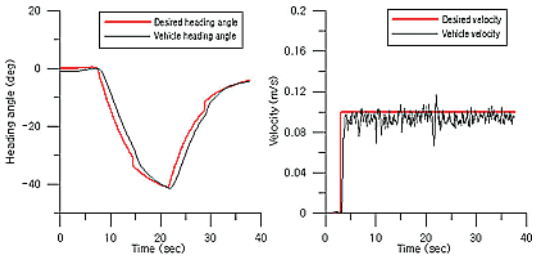

Fig. 13. Experimental results of the heading angle and velocity response for the lane change.

obtained from straight runs, the relationship does not represent the actual relationship for the turning motion of the vehicle. However, because of the experimental difficulties associated with the turning motion, we also used the relation for the turning motion.

Three kinds of tracking maneuvers were tested. The desired forward velocity is 0.1m/sec for all three experiments. The controller gain and LOS values of the three experiments are shown in Table 3.

The first is a lane change maneuver, and the position following the results is shown in Fig. 12. Meanwhile, Fig. 13 shows the heading angle and forward velocity trajectories of the lane change maneuver.
The tracking errors for position, heading, and forward velocity are acceptably small. The second experiment is an obstacle avoidance maneuver or double lane change maneuver. Fig. 14 and Fig. 15 show the mass center, heading angle, and velocity tracking histories for the double lane change. In this case, the lane change gradient is steeper than the previous single lane change. Therefore, the tracking errors of the desired heading angle show larger values.

The third experiment is designed to follow a circular path with a radius of about 1.0 m. Following the circular path is necessary for the vehicle to change direction by 180 degrees. Fig. 16 shows the mass center trajectory. The tracking error slightly increases

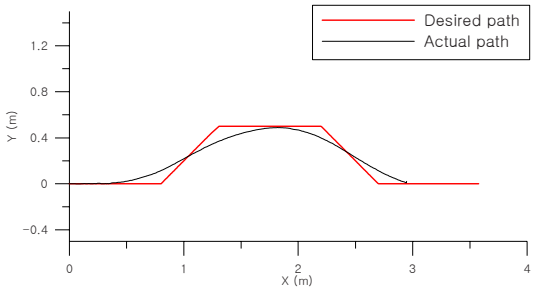

Fig. 14. Vehicle mass center trajectory of the obstacle avoidance experiment.

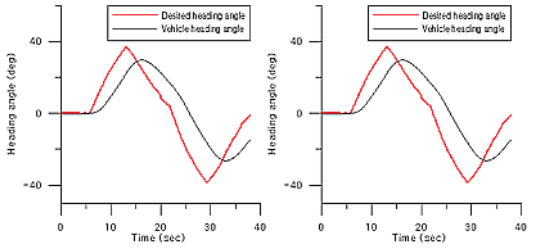

Fig. 15. Experimental results of the heading angle and the velocity response for obstacle avoidance.

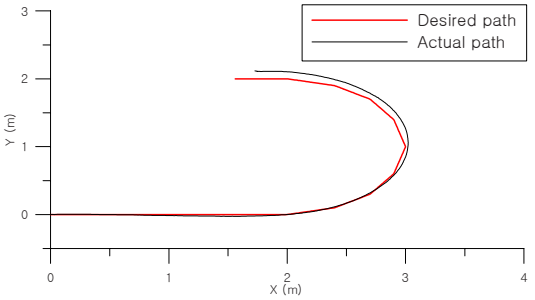

Fig. 16. Vehicle mass center trajectory of the turning experiment.

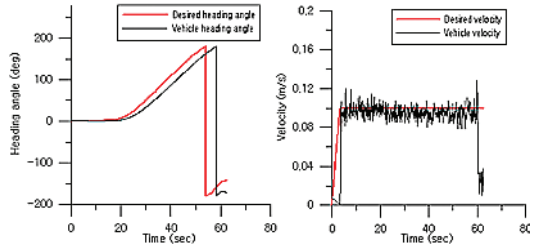

Fig. 17. Results of the heading angle and velocity response for turning.

as the turning progresses. We believe this error was induced by the too soft soil condition on the test bed when the experiment was carried out. If the soil is too soft, the necessary tracking forces from the track cannot be generated.

6. Conclusions

A tracking control algorithm for tracked vehicles operating on an extremely soft soil is developed and verified using a model scale test vehicle. The algorithm consists of a forward velocity control and a desired heading angle control. The desired forward velocity and heading angle are obtained using way points and the LOS concept. The algorithm is designed using kinematics, and it considers the track slips and the nonlinear dynamics of the tracked vehicle.

The experiment results of the lane change and circular turning trajectories show relatively small path tracking errors. Typically, the tracking error for a circular path having a 1.0 m radius would show the maximum error of 0.1 m for the forward vehicle speed of 0.1 m/sec.

As a future work, underwater experiments using a sonar system rather than a vision system are underway. The experiment will utilize an Extended Kalman filter algorithm to reduce sonar noise.

References

[1] S. Hong, H. W. Kim and J. S. Choi, Transient Dynamic Analysis of Tracked Vehicles on Extremely Soft Cohesive Soil, *ISOPE Pacific/Asia Offshore Mechanics Symposium,* (2002) 100-107.

[2] M. Ahmadi, V. Polotski and R. Hurteau, Path Tracking Control of Tracked Vehicles, *IEEE International Conference on Robotics and Automation* 3 (2000) 24-28.

[3] L. Guo, C. C. Kha, H. J. Biao and H. HuiDao, Robust PD control of unmanned land vehicles, *TENCON '93. Proceedings. of Computer, Communication , Control, and Power Engineering*., (1993).

[4] J. Y. Wong, *Theory of Ground Vehicles*, 3rd ed. John Willy & Sons, inc, (2001).

[5] A. T. Le, D. C. Rye and H. F. Durrant-Whyte, Estimation of track-soil interactions for autonomous tracked vehicles, *Proc. IEEE International Conference on Robotics and Automation*, Albuquerque, NM. USA, (1997).

[6] J. J. Soltine and W. Li, *Applied Nonlinear Control*, Prentice Hall International, inc, (1991).

[7] T. I. Fossen, *Marine Control System*, Marine Cybernetics AS, (2002).

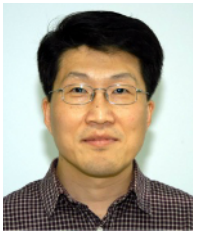

Sup Hong received the B.Sc. and the M.sc. degree in the department of naval architecture and ocean engineering from Seoul National University, Korea, and the Doctor of Engineering degree in mechanical engineering from the Technical university of Aachen, Germany. Currently, he is the principal researcher at MOERI (Maritime and Ocean Engineering Research Institute), Korea. His main research areas include dynamics of marine structure, and development of marine mineral resources. Especially, he is focusing on the development of deep seabed mining technologies since 1994.

Mooncheol Won received the B.Sc. and the M.sc. degree in the department of naval architecture and ocean engineering from Seoul National University, Korea, and the Ph.D. degree in mechanical engineering from the University of California at Berkeley, USA. Currently, he is a professor in the department of mechatronics engineering of Chungnam national university, Korea. His research interests include control of maritime and mechatronics systems, and machine learning applications of robotic systems.